Enhanced Near-Boundary Accuracy in the PIES Method Using a Regularized Integral Identity for Three-Dimensional Potential Problems

Krzysztof Szerszeń [0000-0001-9256-2622] and Eugeniusz Zieniuk [0000-0002-6395-5096]

University of Bialystok, Faculty of Computer Science
15-245 Białystok, Konstantego Ciołkowskiego 1M, Poland
k.szerszen@uwb.edu.pl, e.zieniuk@uwb.edu.pl

Abstract. This study introduces a regularization-based strategy to improve solution accuracy near boundaries within the integral identity associated with the Parametric Integral Equation System (PIES) for three-dimensional potential problems. Accuracy deterioration in near-boundary regions arises from singular behavior of the integrand functions in the underlying integral formulation. The proposed approach employs a suitably constructed regularizing function with optimized coefficients to mitigate these effects. Numerical analysis demonstrates a significant enhancement in solution accuracy. The regularization algorithm is independent of boundary geometry, boundary representation, and imposed boundary conditions, highlighting its generality and wide applicability.

Keywords: Parametric integral equation system (PIES), integral identity regularization, near-boundary evaluation, nearly singular integrals, three-dimensional potential problems

1 Introduction

The Parametric Integral Equation System (PIES) constitutes a computational framework for solving boundary value problems (BVPs), derived from classical Boundary Integral Equations (BIEs), through the analytical incorporation of boundary geometry into the formulation [1]. This approach eliminates the standard discretization required in the Boundary Element Method (BEM) [2], where boundary elements simultaneously represent geometry and approximate boundary variables. In PIES, the geometric description of the boundary is formally decoupled from the approximation of boundary solutions, enabling independent strategies for geometric representation and solution approximation. For three-dimensional problems, the boundary element mesh and nodal discretization used in BEM can be replaced by parametric surface patches, such as Coons, Bézier or NURBS, defined by a finite set of control points. Boundary quantities may then be approximated on individual surface patches, for example using Chebyshev series, allowing systematic control of solution accuracy through adjustment of the number of expansion terms without modifying the geometric representation. As a result, PIES offers a significant advantage over BEM, where accuracy improvement typically

ICCS Camera Ready Version 2026
To cite this paper please use the final published version:
DOI: 10.1007/978-3-032-29921-5_20

requires mesh refinement and redefinition of the boundary using an increased number of elements.

As an analytical modification of BIE, PIES inherently retains the presence of singular boundary integrals [3]. These singularities arise from the dependence of the integrand functions in both BIE and PIES on the distance between the source point and the field point. As this distance approaches zero, undesirable singular behavior occurs, causing the integrand values to become unbounded. To address this issue, several techniques have been developed within the PIES framework, among which regularization methods [4] represent the most recent advancement, enabling efficient evaluation of singular boundary integrals. The PIES solution procedure yields boundary quantities approximated using Chebyshev series expansions. Based on these boundary solutions, field values on the domain can subsequently be computed using the integral identity associated with PIES. However, it should be noted that the computational accuracy deteriorates significantly for points located on the computational domain in the immediate vicinity of the boundary due to the presence of nearly singular integrals within this identity. Similar difficulties are also observed in integral identities associated with classical BIE formulations.

Over the years, numerous approaches have been proposed to address this issue, the majority of which have been developed within the BEM framework. Among them, subdivision methods [5,6] introduce additional discretization by subdividing boundary elements into smaller subelements in regions affected by near singularities. Although this approach improves accuracy, it significantly increases computational cost due to the growth in the number of elements. Another class of techniques relies on the analytical evaluation of nearly singular integrals [7-9]; however, their applicability is typically limited to simple boundary geometries. Specialized Gaussian quadrature schemes designed for nearly singular integrals constitute another commonly used approach [10]. Alternatively, the virtual boundary element method [11,12] introduces an auxiliary virtual boundary with respect to the physical computational domain, thereby avoiding singular behavior in the integrand functions. A limitation of this strategy, however, lies in the appropriate selection of the distance between the real and virtual boundaries. One of the most widely adopted groups of methods involves coordinate transformation techniques, which aim to eliminate or weaken singularities through suitable mappings. Frequently used transformations include polynomial [13], bicubic [14], rational [15], sigmoidal [16], and sinh transformations [17,18]. Despite their popularity, identifying a universal transformation effective for a broad class of nearly singular integrals remains challenging.

In this study, a novel algorithm is proposed to enhance near-boundary solution accuracy for three-dimensional potential problems. The method is based on the regularization of the original nearly singular integral identity, achieved through a suitably constructed regularizing function with carefully selected coefficients. This approach effectively eliminates near-singular behavior from the integrand functions. The proposed algorithm extends previous work on the regularization of the PIES formulation [4]. Its performance is illustrated through benchmark examples, demonstrating the impact of the regularization on improving solution accuracy at points located close to the boundary.

ICCS Camera Ready Version 2026
To cite this paper please use the final published version:
DOI: 10.1007/978-3-032-29921-5_20

2 Formulation of the Singular PIES and Its Corresponding Integral Identity

The general characteristics of PIES and its associated integral identity have been extensively discussed in the literature [1,4]. Only the fundamental assumptions of the method are summarized here. In this study, we consider boundary value problems governed by Laplace's equation, defined within a three-dimensional domain Ω bounded by the boundary Γ. The classical BIE is formulated directly on Γ, which, in computational practice, requires its discretization into a boundary element mesh within the BEM framework. In the PIES approach, the same boundary can be represented using a significantly smaller number of parametric surface patches compared to the number of boundary elements. Figure 1 schematically illustrates the polygonal boundary of a simplified car model, represented using triangular boundary elements in the BEM framework and first-order Bézier surface patches in PIES.

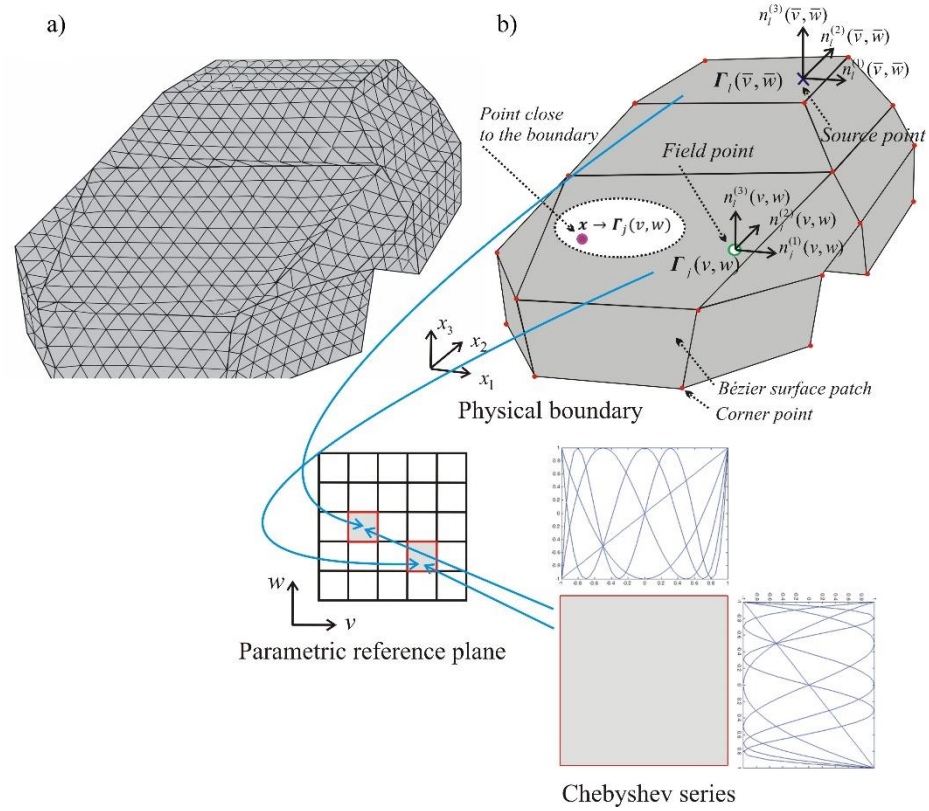

Fig. 1. Boundary discretization with triangular elements in BEM (a) and boundary representation using Bézier surface patches in PIES, mapped onto the parametric plane with Chebyshev-based approximation of boundary values (b).

ICCS Camera Ready Version 2026
To cite this paper please use the final published version:
DOI: 10.1007/978-3-032-29921-5_20

The Bézier surface patches defining the boundary, described by the parametric functions $\boldsymbol{\Gamma}_j(v,w)$, where the index j denotes the patch number, are analytically incorporated into the PIES formulation. For a three-dimensional boundary value problem governed by Laplace's equation, this formulation allows the determination of boundary solutions in the form of the functions $u_j(v,w)$ and $p_j(v,w)$ and can be expressed as follows [1]

$$0.5u_l(\bar{v},\bar{w}) = \sum_{j=1}^{N}\int_{v_{j-1}}^{v_j}\int_{w_{j-1}}^{w_j}\{\bar{U}_{lj}^*(\bar{v},\bar{w},v,w)p_j(v,w) - \bar{P}_{lj}^*(\bar{v},\bar{w},v,w)u_j(v,w)\}J_j(v,w)dvdw, \tag{1}$$

where $v_{j-1} < \bar{v}, v < v_j,\ w_{j-1} < \bar{w}, w < w_j,\ l = 1,2,3,\dots,N.$

The function $u_j(v,w)$ represents the temperature distribution on the boundary, whereas $p_j(v,w)$ denotes the corresponding temperature flux. Once $u_j(v,w)$ and $p_j(v,w)$ are determined, the field distribution $u(\boldsymbol{x})$ at a point $\boldsymbol{x} \in \Omega$ is computed using the following integral identity associated with PIES [1]

$$u(\boldsymbol{x}) = \sum_{j=1}^{N}\int_{v_{j-1}}^{v_j}\int_{w_{j-1}}^{w_j}\{\bar{U}_j^*(\boldsymbol{x},v,w)p_j(v,w) - \bar{P}_j^*(\boldsymbol{x},v,w)u_j(v,w)\}J_j(v,w)dvdw. \tag{2}$$

In the integrand functions of Eq. (1), expressed as

$$\bar{U}_{lj}^*(\bar{v},\bar{w},v,w) = \frac{1}{4\pi}\frac{1}{(\eta_1^2+\eta_2^2+\eta_3^2)^{0.5}}, \tag{3a}$$

$$\bar{P}_{lj}^*(\bar{v},\bar{w},v,w) = \frac{1}{4\pi}\frac{\eta_1 n_j^{(1)}(v,w)+\eta_2 n_j^{(2)}(v,w)+\eta_3 n_j^{(3)}(v,w)}{(\eta_1^2+\eta_2^2+\eta_3^2)^{1.5}}, \tag{3b}$$

and their counterparts in Eq. (2)

$$\bar{U}_j^*(\boldsymbol{x},v,w) = \frac{1}{4\pi}\frac{1}{(\bar{\eta}_1^2+\bar{\eta}_2^2+\bar{\eta}_3^2)^{0.5}}, \tag{4a}$$

$$\bar{P}_j^*(\boldsymbol{x},v,w) = \frac{1}{4\pi}\frac{\bar{\eta}_1 n_j^{(1)}(v,w)+\bar{\eta}_2 n_j^{(2)}(v,w)+\bar{\eta}_3 n_j^{(3)}(v,w)}{(\bar{\eta}_1^2+\bar{\eta}_2^2+\bar{\eta}_3^2)^{1.5}}, \tag{4b}$$

the boundary is analytically incorporated via the parametric functions $\boldsymbol{\Gamma}_j(v,w)$ defining the set of parametric surface patches, according to

$$\eta_1 = \Gamma_l^{(1)}(\bar{v},\bar{w}) - \Gamma_j^{(1)}(v,w), \eta_2 = \Gamma_l^{(2)}(\bar{v},\bar{w}) - \Gamma_j^{(2)}(v,w), \eta_3 = \Gamma_l^{(3)}(\bar{v},\bar{w}) - \Gamma_j^{(3)}(v,w), \tag{5}$$

$$\bar{\eta}_1 = x_1 - \Gamma_j^{(1)}(v,w), \bar{\eta}_2 = x_2 - \Gamma_j^{(2)}(v,w), \bar{\eta}_3 = x_3 - \Gamma_j^{(3)}(v,w), \tag{6}$$

where $\Gamma_j^{(1)}(v,w)$, $\Gamma_j^{(2)}(v,w)$, $\Gamma_j^{(3)}(v,w)$ are the scalar components of the patch function $\boldsymbol{\Gamma}_j(v,w)$ defined on the parametric reference plane with parameters v and w. Similarly, $\Gamma_l^{(1)}(\bar{v},\bar{w})$, $\Gamma_l^{(2)}(\bar{v},\bar{w})$, $\Gamma_l^{(3)}(\bar{v},\bar{w})$ represent the scalar components of the l-th patch function specifying the position $(\bar{v},\bar{w})$ of the source point on the parametric reference plane. They are shown schematically in Figure 1b. Furthermore, $n_j^{(1)}(v,w)$, $n_j^{(2)}(v,w), n_j^{(3)}(v,w)$ denote the components of the normal vector $\boldsymbol{n}_j(v,w)$ at the

ICCS Camera Ready Version 2026
To cite this paper please use the final published version:
DOI: 10.1007/978-3-032-29921-5_20

boundary, while $J_j(v,w)$ represents the Jacobian of the mapping between the Cartesian coordinates and the parametric reference plane. Consequently, both the PIES defined by Eq. (1) and its associated integral identity in Eq. (2) are not formulated directly on the physical boundary, but on the parametric reference plane, as illustrated in Figure 1b.

Due to the nature of Eq. (1), the integrand functions in (3a,b) exhibit singular behavior. Their regularization was proposed in [4], effectively eliminating these singularities. However, when evaluating solutions at points near the boundary, i.e., as $\boldsymbol{x} \to \boldsymbol{\Gamma}_j(v,w)$ (schematically shown in Figure 1b), the integrand functions in (4a,b) within identity (2), similar to the classical BIE approach, exhibit nearly singular behavior. This implies that, although the nearly singular integrals are theoretically regular and finite, their behavior near the boundary closely resembles that of true singular integrals, leading to a reduction in solution accuracy at points adjacent to the boundary. The objective of this study is to eliminate the nearly singular character of these integrand functions. This will be achieved through the regularization of the formula (2), which is presented in the following section.

3 Regularization of the Integral Identity

The regularization procedure begins with the definition of the auxiliary function $\hat{u}_j(\boldsymbol{x})$, for $\boldsymbol{x} \in \Omega$, as follows

$$\hat{u}_j(\boldsymbol{x}) = A_l(\bar{v},\bar{w})(\boldsymbol{x} - \boldsymbol{\Gamma}_l(\bar{v},\bar{w})) + B_l(\bar{v},\bar{w}). \tag{7}$$

The function (7) satisfies the Laplace equation and is hereafter referred to as the regularizing function. It contains two unknown coefficients, $A_l(\bar{v},\bar{w})$ and $B_l(\bar{v},\bar{w})$. From (7), the expression for $\hat{u}_j(v,w)$, when $\boldsymbol{x} \in \boldsymbol{\Gamma}_j(v,w)$ is obtained as follows

$$\hat{u}_j(v,w) = A_l(\bar{v},\bar{w})(\boldsymbol{\Gamma}_j(v,w) - \boldsymbol{\Gamma}_l(\bar{v},\bar{w})) + B_l(\bar{v},\bar{w}). \tag{8}$$

Moreover, $\hat{p}_j(v,w)$ denotes the normal derivative of (8) with respect to the boundary normal vector $\boldsymbol{n}_j(v,w)$ and is expressed as follows

$$\hat{p}_j(v,w) = A_l(\bar{v},\bar{w})\boldsymbol{n}_j(v,w). \tag{9}$$

In the subsequent step, (7)-(9) are substituted into Eq. (2), as follows

$$\hat{u}(\boldsymbol{x}) = \sum_{j=1}^{N} \int_{v_{j-1}}^{v_j} \int_{w_{j-1}}^{w_j} \{\bar{U}_j^*(\boldsymbol{x},v,w)\hat{p}_j(v,w) - \bar{P}_j^*(\boldsymbol{x},v,w)\hat{u}_j(v,w)\} J_j(v,w)\,dv\,dw. \tag{10}$$

The functions $\hat{u}_j(v,w)$ and $\hat{p}_j(v,w)$ in Eq. (10) are defined within the parametric reference plane (v,w), whereas $\hat{u}(\boldsymbol{x})$ is defined for $\boldsymbol{x} \in \Omega$. Substituting Eqs. (7)–(9) into Eq. (10) yields

$$A_l(\bar{v},\bar{w})(\boldsymbol{x} - \boldsymbol{\Gamma}_l(\bar{v},\bar{w})) + B_l(\bar{v},\bar{w}) = \sum_{j=1}^{N} \int_{v_{j-1}}^{v_j} \int_{w_{j-1}}^{w_j} \{\bar{U}_j^*(\boldsymbol{x},v,w)A_l(\bar{v},\bar{w})\boldsymbol{n}_j(v,w) - \bar{P}_j^*(\boldsymbol{x},v,w)[A_l(\bar{v},\bar{w})(\boldsymbol{\Gamma}_j(v,w) - \boldsymbol{\Gamma}_l(\bar{v},\bar{w})) + B_l(\bar{v},\bar{w})]\} J_j(v,w)\,dv\,dw. \tag{11}$$

ICCS Camera Ready Version 2026
To cite this paper please use the final published version:
DOI: 10.1007/978-3-032-29921-5_20

Next, subtracting Eq. (11) from the original integral identity (2) and applying appropriate simplifications yields

$$u(\boldsymbol{x}) - A_l(\bar{v},\bar{w})(\boldsymbol{x} - \boldsymbol{\Gamma}_l(\bar{v},\bar{w})) - B_l(\bar{v},\bar{w}) = \sum_{j=1}^{N}\int_{v_{j-1}}^{v_j}\int_{w_{j-1}}^{w_j}\{\bar{U}_j^*(\boldsymbol{x},v,w)\big[p_j(v,w) - A_l(\bar{v},\bar{w})\boldsymbol{n}_j(v,w)\big] - \bar{P}_j^*(\boldsymbol{x},v,w)\big[u_j(v,w) - A_l(\bar{v},\bar{w})(\boldsymbol{\Gamma}_j(v,w) - \boldsymbol{\Gamma}_l(\bar{v},\bar{w})) - B_l(\bar{v},\bar{w})\big]\}J_j(v,w)dvdw. \quad (12)$$

The coefficient $A_l(\bar{v},\bar{w})$ is introduced to regularize the first integral in Eq. (12), whereas $B_l(\bar{v},\bar{w})$ regularizes the second integral in the same expression. To ensure that the integral functions $\bar{U}_j^*(\boldsymbol{x},v,w)$ and $\bar{P}_j^*(\boldsymbol{x},v,w)$ remain non-singular as the point $\boldsymbol{x}$ approaches the boundary Γ from the domain Ω, these coefficients must assume the following forms

$$A_l(\bar{v},\bar{w}) = \frac{p_l(\bar{v},\bar{w})}{n_l^{(1)}(\bar{v},\bar{w}) + n_l^{(2)}(\bar{v},\bar{w}) + n_l^{(3)}(\bar{v},\bar{w})}, \quad (13a)$$

$$B_l(\bar{v},\bar{w}) = u_l(\bar{v},\bar{w}). \quad (13b)$$

Finally, upon substituting (13a,b) into Eq. (12), the resulting expression yields the final, regularized form of the integral identity, given as follows

$$u(\boldsymbol{x}) = A_l(\bar{v},\bar{w})(\boldsymbol{x} - \boldsymbol{\Gamma}_l(\bar{v},\bar{w})) + B_l(\bar{v},\bar{w}) + \sum_{j=1}^{N}\int_{v_{j-1}}^{v_j}\int_{w_{j-1}}^{w_j}\{\bar{U}_j^*(\boldsymbol{x},v,w)\big[p_j(v,w) - d_{lj}(v,w,\bar{v},\bar{w})p_l(\bar{v},\bar{w})\big] - \bar{P}_j^*(\boldsymbol{x},v,w)[u_j(v,w) - u_l(\bar{v},\bar{w}) - g_{lj}(v,w,\bar{v},\bar{w})p_l(\bar{v},\bar{w})]\}J_j(v,w)dvdw, \quad (14)$$

where

$$d_{lj}(v,w,\bar{v},\bar{w}) = \frac{n_j^{(1)}(v,w) + n_j^{(2)}(v,w) + n_j^{(3)}(v,w)}{n_l^{(1)}(\bar{v},\bar{w}) + n_l^{(2)}(\bar{v},\bar{w}) + n_l^{(3)}(\bar{v},\bar{w})}, \quad (15)$$

$$g_{lj}(v,w,\bar{v},\bar{w}) = \frac{\left(\Gamma_j^{(1)}(v,w) - \Gamma_l^{(1)}(\bar{v},\bar{w})\right) + \left(\Gamma_j^{(2)}(v,w) - \Gamma_l^{(2)}(\bar{v},\bar{w})\right) + \left(\Gamma_j^{(3)}(v,w) - \Gamma_l^{(3)}(\bar{v},\bar{w})\right)}{n_l^{(1)}(\bar{v},\bar{w}) + n_l^{(2)}(\bar{v},\bar{w}) + n_l^{(3)}(\bar{v},\bar{w})}. \quad (16)$$

The formula $d_{lj}(\bar{v},\bar{w},v,w)$ regularizes $\bar{U}_j^*(\boldsymbol{x},v,w)$ exhibiting a quasi-weak singularity, whereas $g_{lj}(\bar{v},\bar{w},v,w)$ is responsible for the regularization of $\bar{P}_j^*(\boldsymbol{x},v,w)$ with a quasi-strong singularity. Formulas (15) and (16) are valid for problems in which the sum of the components of the normal vector $n_l^{(1)}(\bar{v},\bar{w}) + n_l^{(2)}(\bar{v},\bar{w}) + n_l^{(3)}(\bar{v},\bar{w})$ for the patch $\boldsymbol{\Gamma}_l(\bar{v},\bar{w})$ is non-zero.

4 Numerical implementation

To determine the solution at points $\boldsymbol{x} \in \Omega$ using Eq. (14), it is first necessary to evaluate the boundary solutions, represented by $u_j(v,w)$ and $p_j(v,w)$. Although Eg. (1) can be used for this purpose, it leads to the occurrence of singular integrals. A more effective approach is to employ a modified version of Eq. (1), derived in [4], which can be written in the following form

ICCS Camera Ready Version 2026
To cite this paper please use the final published version:
DOI: 10.1007/978-3-032-29921-5_20

$$\sum_{j=1}^{N}\Big\{\int_{v_{j-1}}^{v_j}\int_{w_{j-1}}^{w_j}\bar{U}_{lj}^{*}(\bar{v},\bar{w},v,w)\big[p_j(v,w)-d_{lj}(\bar{v},\bar{w},v,w)p_l(\bar{v},\bar{w})\big]-\int_{v_{j-1}}^{v_j}\int_{w_{j-1}}^{w_j}\bar{P}_{lj}^{*}(\bar{v},\bar{w},v,w)[u_j(v,w)-u_l(\bar{v},\bar{w})-g_{lj}(\bar{v},\bar{w},v,w)p_l(\bar{v},\bar{w})]\Big\}J_j(v,w)dvdw=0, \tag{17}$$

where $v_{j-1}<\bar{v},v<v_j,\ w_{j-1}<\bar{w},w<w_j,\ l=1,2,3,\dots,N.$

Equation (17) represents a regularized form of Eq. (1), in which the singularities have been removed. It incorporates the same regularization functions as those defined in (15) and (16). Consistent with previous studies, the boundary functions $u_j(v,w)$ and $p_j(v,w)$ on each patch are approximated using a tensor product of two one-dimensional Chebyshev series, as shown below

$$u_j(v,w)=\sum_{p=0}^{P-1}\sum_{r=0}^{R-1}u_j^{(pr)}T_j^{(p)}(v)T_j^{(r)}(w), \tag{18}$$

$$p_j(v,w)=\sum_{p=0}^{P-1}\sum_{r=0}^{R-1}p_j^{(pr)}T_j^{(p)}(v)T_j^{(r)}(w), \tag{19}$$

where $u_j^{(pr)}$ and $p_j^{(pr)}$ denote the coefficients obtained by enforcing the boundary conditions or by solving the boundary value problem using the regularized PIES formulation given in Eq. (17). Substituting Eqs. (18) and (19) into Eq. (17) then yields

$$\sum_{j=1}^{N}\{\sum_{p=0}^{P-1}\sum_{r=0}^{R-1}\int_{v_{j-1}}^{v_j}\int_{w_{j-1}}^{w_j}\bar{U}_{lj}^{*}(\bar{v},\bar{w},v,w)\,[p_j^{(pr)}T_j^{(p)}(v)T_j^{(r)}(w)-d_{lj}(v,w,\bar{v},\bar{w})p_l^{(pr)}T_l^{(p)}(\bar{v})T_l^{(r)}(\bar{w})]-\sum_{p=0}^{P-1}\sum_{r=0}^{R-1}\int_{v_{j-1}}^{v_j}\int_{w_{j-1}}^{w_j}\bar{P}_{lj}^{*}(\bar{v},\bar{w},v,w)\,[u_j^{(pr)}T_j^{(p)}(v)T_j^{(r)}(w)-u_l^{(pr)}T_l^{(p)}(\bar{v})T_l^{(r)}(\bar{w})-g_{lj}(v,w,\bar{v},\bar{w})p_l^{(pr)}T_l^{(p)}(\bar{v})T_l^{(r)}(\bar{w})]\}J_j(v,w)dvdw, \tag{20}$$

where $v_{j-1}<\bar{v},v<v_j,\ w_{j-1}<\bar{w},w<w_j,\ l=1,2,3,\dots,N.$

Equation (20) can be solved using the collocation method. The collocation points are distributed over the parametric reference domain of the individual surface patches, defined by the parameters $\bar{v}$ and $\bar{w}$. Evaluating Eq. (20) at these points leads to a system of algebraic equations, the size of which depends on the number of Bézier patches N and the number of coefficients $P\times R$ in the series (18) and (19) associated with each patch.

In the second step, these expressions are used to approximate the boundary functions in Eq. (14), yielding the following

$$u(\boldsymbol{x})=\frac{\boldsymbol{x}-\Gamma_l(\bar{v},\bar{w})}{n_l^{(1)}(\bar{v},\bar{w})+n_l^{(2)}(\bar{v},\bar{w})+n_l^{(3)}(\bar{v},\bar{w})}p_l(\bar{v},\bar{w})+u_l(\bar{v},\bar{w})+\sum_{j=1}^{N}\{\sum_{p=0}^{P-1}\sum_{r=0}^{R-1}\int_{v_{j-1}}^{v_j}\int_{w_{j-1}}^{w_j}\bar{U}_j^{*}(\boldsymbol{x},v,w)\,[p_j^{(pr)}T_j^{(p)}(v)T_j^{(r)}(w)-d_{lj}(v,w,\bar{v},\bar{w})p_l^{(pr)}T_l^{(p)}(\bar{v})T_l^{(r)}(\bar{w})]-\sum_{p=0}^{P-1}\sum_{r=0}^{R-1}\int_{v_{j-1}}^{v_j}\int_{w_{j-1}}^{w_j}\bar{P}_j^{*}(\boldsymbol{x},v,w)\,[u_j^{(pr)}T_j^{(p)}(v)T_j^{(r)}(w)-u_l^{(pr)}T_l^{(p)}(\bar{v})T_l^{(r)}(\bar{w})-g_{lj}(v,w,\bar{v},\bar{w})p_l^{(pr)}T_l^{(p)}(\bar{v})T_l^{(r)}(\bar{w})]\}J_j(v,w)dvdw. \tag{21}$$

ICCS Camera Ready Version 2026
To cite this paper please use the final published version:
DOI: 10.1007/978-3-032-29921-5_20

Identity (21), similarly to Eq. (20), provides an analytical representation of the boundary defined by the surface patches. The procedure for solving the regularized identity in Eq. (21) is outlined below.

Algorithm

To compute the solution at a point $\boldsymbol{x} \in \Omega$ using the regularized integral identity:

- Read the boundary input data, i.e., the control points of the N Bézier patches
- Obtain the coefficients $u_j^{(pr)}$ and $p_j^{(pr)}$ in (18) and (19), determined either by enforcing the boundary conditions or by solving the boundary value problem based on Eq. (17)
- Identify the index l of the surface patch closest to the point $x \in \Omega$

for $p \leftarrow 0, P-1$ **do** *//loop over Chebyshev series*
 for $r \leftarrow 0, R-1$ **do**
  $u(\boldsymbol{x}) = p_l(\bar{v},\bar{w})(\boldsymbol{x} - \boldsymbol{\Gamma}_l(\bar{v},\bar{w}))/n_l^{(1)}(\bar{v},\bar{w}) + n_l^{(2)}(\bar{v},\bar{w}) + n_l^{(3)}(\bar{v},\bar{w}) + u_l(\bar{v},\bar{w})$
 end for
end for

for $l \leftarrow 1, N$ **do** *//loop over Bézier surfaces*
 for $j \leftarrow 1, N$ **do**
  for $p \leftarrow 0, P-1$ **do** *//loop over Chebyshev series*
   for $r \leftarrow 0, R-1$ **do**
   $u(\boldsymbol{x})+$
   $= Gaussian\_integration\big(\bar{U}_j^*(\boldsymbol{x},v,w)[p_j^{(pr)}T_j^{(p)}(v)T_j^{(r)}(w) - d_{lj}(v,w,\bar{v},\bar{w})p_l^{(pr)}T_l^{(p)}(\bar{v})T_l^{(r)}(\bar{w})]\big)$
   $- Gaussian\_integration\big(\bar{P}_j^*(\boldsymbol{x},v,w)[u_j^{(pr)}T_j^{(p)}(v)T_j^{(r)}(w) - u_l^{(pr)}T_l^{(p)}(\bar{v})T_l^{(r)}(\bar{w})$
   $- g_{lj}(v,w,\bar{v},\bar{w})p_l^{(pr)}T_l^{(p)}(\bar{v})T_l^{(r)}(\bar{w})]\big)$
    end for
  end for
 end for
end for

---

5 Impact of regularization on solution accuracy

5.1 Example 1

In the first example, we compare the accuracy of the solutions obtained using the proposed regularization with the results obtained via an alternative method for improving solution accuracy near the boundary, based on the sinh coordinate transformation presented in [18]. The comparative analysis is conducted for the following boundary-value problem of the potential, defined in the domain bounded by a torus centered at the origin, with outer and inner radii of $R = 3$ and $r = 1$, respectively. The prescribed potential distribution on the boundary is given by

$$u(x_1, x_2, x_3) = x_1^2 - x_3^2 + x_1x_2 + x_2x_3 - 2 + x_1 + 1. \tag{22}$$

ICCS Camera Ready Version 2026
To cite this paper please use the final published version:
DOI: 10.1007/978-3-032-29921-5_20

For the sinh method, this boundary-value problem was solved using the BEM, with the torus boundary discretized into 80 quadratic quadrilateral boundary elements. For the PIES approach, the same boundary is represented by 16 cubic Bézier surface patches. A comparison of solution accuracy, based on the computed relative errors for the potential $u(x_1, x_2, x_3)$ at interior points along the x_1-axis, obtained using both the sinh method and the proposed regularization, is presented in Table 1.

Table 1. Comparison of relative errors in solutions obtained with the sinh-transformation method and the proposed regularization approach.

Interior points	Exact (22)	Relative error	
		Identity (14)	sinh [18]
(2.0001, 0, 0)	1.007666	8.71897 E–04	4.046417E–03
(2.001, 0, 0)	1.009474	8.12282 E–04	4.035724E–03
(2.01, 0, 0)	1.027640	4.49495 E–04	3.926795E–03
(2.1, 0, 0)	1.218210	5.63306 E–04	2.782792E–03
(2.2, 0, 0)	1.440000	3.62021 E–04	1.763063E–03
(2.6, 0, 0)	2.560000	2.81491 E–05	1.794608E–03
(3.0, 0, 0)	4.000000	2.13806 E–05	1.094613E–03

As shown in Table 1, the results obtained using identity (14) demonstrate good accuracy throughout the analyzed section. These results were computed using $P = R = 5$ terms of the Chebyshev series for each of the 16 Bézier patches. Moreover, the presented approach yields higher accuracy compared to the sinh-transformation method.

5.2 Example 2

The effectiveness of the proposed approach is assessed by evaluating the solution at points located in the immediate vicinity of the boundary. The analysis is performed for a closed boundary resembling a simplified car model, as shown in Figure 2. The boundary is formed by 22 linear Bézier patches.

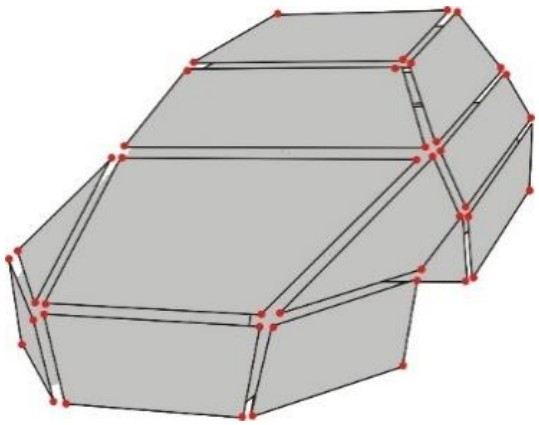

Fig. 2. Boundary representation of the simplified car model used in the analysis, showing the local corner points of the patches.

ICCS Camera Ready Version 2026
To cite this paper please use the final published version:
DOI: 10.1007/978-3-032-29921-5_20

The desired field distribution on the boundary and within the domain is assumed to be a function of the Cartesian coordinates $\boldsymbol{x} = \{x_1, x_2, x_3\}$, as defined below

$$u(x_1, x_2, x_3) = 2x_1^2 + 2x_2^2 - x_3^2. \tag{23}$$

Dirichlet boundary conditions are prescribed on each boundary patch using this function, which also represents the analytical solution within the domain and serves as a reference for evaluating the results.

To obtain the solution within the domain, the first stage involves determining the boundary solution for the prescribed boundary shape and boundary conditions using Eq. (20) via the collocation method. The boundary solution is approximated with Chebyshev series, using $P = R = 5$ terms for each component patch of the boundary. The resulting series coefficients are then employed in Eqs. (2) and (14) to compute $u(\boldsymbol{x})$ at points within the domain $\boldsymbol{x} \in \Omega$, including those in the immediate vicinity of the boundary. Table 2 presents the mean squared percentage error for solutions evaluated at 2,200 points near the boundary using Eqs. (2) and (14), with respect to the reference solution (19). Six variants of test-point distances from the boundary are considered, ranging from from 1e-1 to 1e-6.

Table 2. Mean squared percentage error as a function of the distance of test points from the boundary.

Distance	(2)	(14)
1e-6	50.6383	1.8555e-6
1e-5	50.3567	1.4323e-5
1e-4	50.1262	1.4439e-4
1e-3	47.6855	1.2376e-3
1e-2	24.6363	4.3773e-3
1e-1	0.00027	1.0601e-5

The results show that solutions based on the unregularized integral identity (2) exhibit substantially lower accuracy than those obtained using identity (14). The regularized identity (14) reduces the error by approximately five orders of magnitude, significantly enhancing solution accuracy near the boundary and enabling effective adaptation to varying distances of computational points from the boundary. To illustrate the results summarized in Table 1, Figure 3 shows the distributions of relative percentage errors at selected points in the immediate vicinity of the boundary for 1e-6.

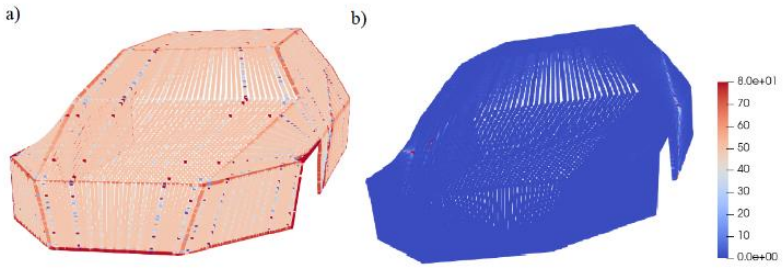

Fig. 3. Error distribution for solutions in the domain located at a distance of 1e-6 from the boundary, obtained using (a) identity (2) and (b) identity (14).

ICCS Camera Ready Version 2026
To cite this paper please use the final published version:
DOI: 10.1007/978-3-032-29921-5_20

Figure 3 shows that the applied regularization procedure enables accurate computation of the solution in the immediate vicinity of the boundary, with errors below 1% at points located 1e-6 from the boundary. By contrast, the singular identity (2) yields substantially larger errors, reaching up to 80% at points at the same distance.

6 Conclusion

This work introduces a modified form of the integral identity in the PIES method, effectively eliminating singularities and improving solution accuracy in regions near the boundary. This approach overcomes a major limitation of both the classical BIE and the unregularized identity (2) when computing solutions in regions adjacent to the boundary.

The regularization maintains a formal separation between the boundary geometry description and the approximation of boundary functions, enabling the continued use of Chebyshev series for approximation. The strategy is independent of both the boundary parameterization and the type of boundary conditions, confirming its general applicability. In the present study, the boundary is defined using first-order rectangular Bézier surface patches, but it can be represented using higher-order Bézier patches or other surfaces, such as B-splines or NURBS. Crucially, the proposed regularization substantially enhances solution accuracy near the boundary, addressing a fundamental challenge in integral methods for solving boundary value problems.

In the next stage of the research, the computational complexity of the proposed regularization will be analyzed, along with further development of the method for boundary value problems governed by other classes of differential equations, such as those arising in linear elasticity.

References

1. Zieniuk, E. (2013). Computational method PIES for solving boundary value problems. PWN, Warsaw.
2. Brebbia, C. A., Telles, J. C. F., Wrobel, L. C. (2012). Boundary element techniques: theory and applications in engineering. Springer Science & Business Media.
3. Hsiao, G. C., Wendland, W. L. (2021). Boundary integral equations. Springer Berlin Heidelberg.
4. Szerszeń, K., Eugeniusz Z. (2024). Elimination of computing singular surface integrals in the PIES method through regularization for three-dimensional potential problems. International Conference on Computational Science. Cham: Springer Nature Switzerland.
5. Zhang, J., Ju, C., Divo, E., Zhong, Y., Chi, B. (2019). A binary-tree subdivision method for evaluation of singular integrals in 3D BEM. Engineering Analysis with Boundary Elements, 103, 80-93.
6. Qu, S., Chen, H., & Li, S. (2014). Adaptive integration method based on sub-division technique for nearly singular integrals in near-field acoustics boundary element analysis. Journal of Low Frequency Noise, Vibration and Active Control, 33(1), 27-45.
7. Ren, Q., Chan, C. L. (2015). Analytical evaluation of the BEM singular integrals for 3D Laplace and Stokes flow equations using coordinate transformation. Engineering Analysis with Boundary Elements, 53, 1-8.

ICCS Camera Ready Version 2026
To cite this paper please use the final published version:
DOI: 10.1007/978-3-032-29921-5_20

8. Zhou, H., Niu, Z., Cheng, C., Guan, Z. (2008). Analytical integral algorithm applied to boundary layer effect and thin body effect in BEM for anisotropic potential problems. Computers & Structures, 86(15-16), 1656-1671.
9. Han, Z., Pan, W., Cheng, C., Hu, Z., & Niu, Z. (2022). A semi-analytical treatment for nearly singular integrals arising in the isogeometric boundary element method-based solutions of 3D potential problems. Computer Methods in Applied Mechanics and Engineering, 398, 115179.
10. Tausch, J. (2022). Adaptive quadrature rules for Galerkin BEM. Computers & Mathematics with Applications, 113, 270-281.
11. Li, X. C., Yao, W. A. (2006). Virtual boundary element-integral collocation method for the plane magnetoelectroelastic solids. Engineering Analysis with Boundary Elements, 30(8), 709-717.
12. Weian, Y., Wang, H. (2005). Virtual boundary element integral method for 2-D piezoelectric media. Finite Elements in Analysis and Design, 41(9-10), 875-891.
13. Telles, J. (1987). A self-adaptive co-ordinate transformation for efficient numerical evaluation of general boundary element integrals. International Journal for Numerical Methods in Engineering, 24(5), 959-973.
14. Cerrolaza, M., Alarcon, E. (1989). A bi-cubic transformation for the numerical evaluation of the Cauchy principal value integrals in boundary methods. International Journal for Numerical Methods in Engineering, 28(5), 987-999.
15. Huang, Q., Cruse, T. (1993). Some notes on singular integral techniques in boundary element analysis. International Journal for Numerical Methods in Engineering, 36(15), 2643-2659.
16. Wang, H., Chen, Y., Sun, S., & Hu, J. (2024). A New Sigmoidal Transformation for Strongly Near-Singular Integrals Over Triangular Elements. IEEE Antennas and Wireless Propagation Letters, 23(7), 1981-1985.
17. Zhang, J., Chi, B., Singh, K. M., Zhong, Y., & Ju, C. (2019). A binary-tree element subdivision method for evaluation of nearly singular domain integrals with continuous or discontinuous kernel. Journal of Computational and Applied Mathematics, 362, 22-40.
18. Li, X., Zhang, Y., Gong, Y., Su, Y., & Gao, X. (2015). Use of the sinh transformation for evaluating 2D nearly singular integrals in 3D BEM. Acta Mechanica, 226(9), 2873-2885.

ICCS Camera Ready Version 2026
To cite this paper please use the final published version:
DOI: 10.1007/978-3-032-29921-5_20